Monte Carlo simulation of phase separation during thin-film codeposition

C. D. Adams and D. J. Srolovitz
Department of Materials Science and Engineering, University of Michigan, Ann Arbor, Michigan 48109-2136

M. Atzmon
Department of Nuclear Engineering, University of Michigan, Ann Arbor, Michigan 48109-2104

(Received 4 January 1993; accepted for publication 17 April 1993)

The results of Monte Carlo simulation of phase separation during binary film coevaporation are presented for a range of deposition conditions. The model employed assumes that phase separation occurs through surface interdiffusion during deposition, while the bulk of the film remains frozen. Simulations were performed on A-B alloy films having compositions of 10 and 50 vol % solute. For both film compositions, the lateral scale of the domains at the film surface evolves to a steady-state size during deposition. A power-law dependence of the steady-state domain size on the inverse deposition rate is obtained. Simulation microstructures at 50 vol % compare favorably with those obtained in a previous experimental study of phase separation during coevaporation of Al-Ge films of the same composition. Results of simulations performed at 10 vol % are compared with the predictions of a theoretical model based on the above assumptions. The power-law exponent obtained from simulations at 10 vol % is different than that predicted by the theoretical model. The reasons for this difference are discussed.

I. INTRODUCTION

The strong influences of material processing parameters on microstructure development, and of microstructure on the macroscopic properties of bulk and thin-film materials, are well known.[1] For thin films, substrate temperature and deposition rate are two easily accessible deposition parameters influencing microstructure development. There have been numerous investigations of this relationship for single-phase thin films,[2–10] however, there has been little work addressing the influence of deposition parameters on the microstructure and phase morphology of multicomponent thin films. We present here the results of a Monte Carlo computer simulation of phase separation during binary film codeposition for a variety of deposition conditions.

One of the earliest investigations of the relationship between thin-film deposition conditions and microstructure was the work of Movchan and Demchishin[2] on elemental metal and metal oxide films. These authors identified three distinct microstructural zones as a function of the homologous deposition temperature T/T_m, where T is the absolute deposition temperature and T_m is the absolute melting temperature of the deposited material. Zone-I films ($T/T_m < 0.3$) consist of tapered grains separated by regions of porous material, zone-II films ($0.3 < T/T_m < 0.5$) of columnar grains separated by distinct boundaries and zone-III films ($T/T_m > 0.5$) of equiaxed grains separated by distinct boundaries. This work was later expanded upon by Thornton[3,4] to consider the effect of gas pressure on microstructure development in sputter-deposited metal films.

More recently, a number of investigators have applied Monte Carlo[5–8] and molecular dynamics[9,10] simulation techniques to study the relationship between single-phase thin-film microstructure development and deposition conditions. For example, Müller[9] used molecular dynamics to study the zone-I/zone-II microstructural transition and found that six decades of deposition rate variation can lead to a two-decade variation in the transition temperature. In addition, Srolovitz and co-workers[5,6] and Ling and Anderson[8] used Monte Carlo simulation methods, similar to those employed herein, to study the kinetics of grain coarsening and columnar microstructure evolution in thin films deposited under zone-II deposition conditions. Srolovitz and co-workers[5] also correctly predict the onset of the zone-I/zone-II microstructural transition and account for the grain-size evolution with increasing film thickness observed experimentally.

The model of Movchan and Demchishin,[2] while it agrees with reported experiments[3,4] and simulations[5,6,10] of single-phase thin-film microstructural development, is not applicable to the phase separating multicomponent thin films considered here. Unlike grain coarsening in single-phase films, phase separation is controlled by long-range diffusion. Although phase separation in bulk multicomponent materials has received considerable attention,[1] its treatment is not applicable to phase separation during film growth, where the influence of an externally controlled deposition rate must be considered. Atzmon, Kessler, and Srolovitz[11] have recently developed a theoretical model for surface interdiffusion controlled phase separation during film growth. The main features of that model are similar to those found in Cahn's analysis[12] of eutectoid decomposition of bulk materials.

Our previous experimental observations of coevaporated Al-Ge thin films confirm the strong influence of deposition temperature on phase separation during deposition.[13] The Al-Ge system has a simple eutectic phase diagram with terminal phases that have limited solid solubilities. Therefore, coevaporated films with a composition within the two-phase region of the phase diagram are ex-

 0021-8979/93/74(3)/1707/9/$6.00

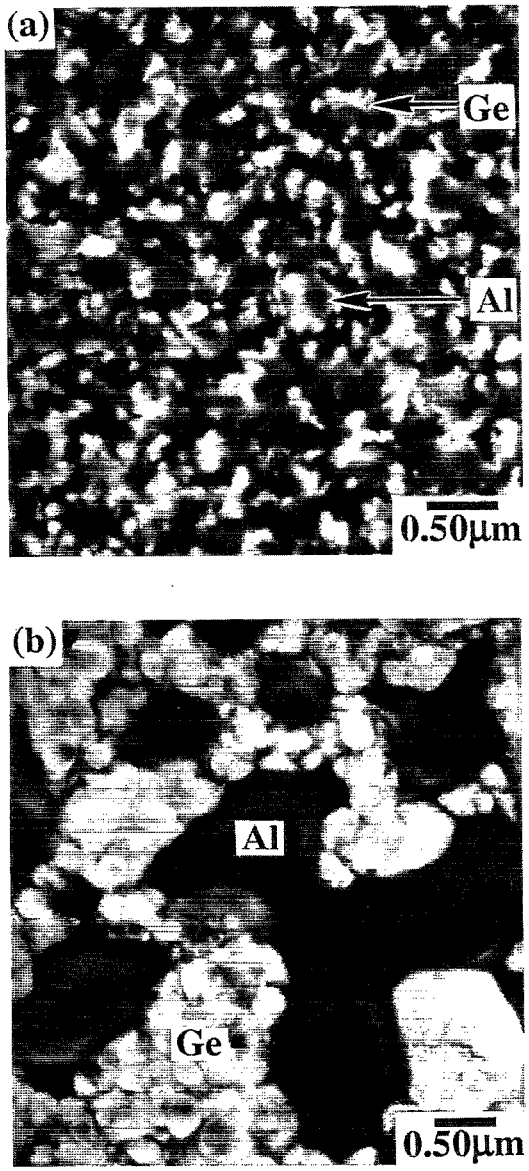

FIG. 1. Secondary electron SEM photomicrographs of the surfaces of coevaporated Al-Ge thin films deposited at (a) 200 °C and (b) 375 °C having thicknesses of 110 and 300 nm, respectively.

pected to phase separate into a mixture of the terminal solid solutions during deposition. We codeposited such films with a composition of 40 at. % (50 vol %) Ge at temperatures between 25 and 375 °C. The microstructures obtained were phase separated, although the phases present were not always the thermodynamically stable phases expected from the equilibrium phase diagram. Two examples of the phase morphologies observed for deposition at 200 and 375 °C are shown in the scanning electron microscopy (SEM) photomicrographs presented in Figs. 1(a) and 1(b), respectively. For both deposition temperatures one observes, at the film surfaces, a mixture of intertwined domains of the Al- and Ge-rich terminal phases. The characteristic length scale of the domains is ~300 nm in the film deposited at 200 °C and ~700 nm in the film deposited at 375 °C. The variation in this domain size with deposition temperature exhibited Arrhenius behavior and the associated activation energy was found to be consistent with surface interdiffusion-controlled phase separation.[13]

In this article, we present the results of a Monte Carlo simulation of phase separation during codeposition of binary thin films. The simulation procedure explicitly considers the case of a binary alloy system with terminal phases that have limited solubilities such that phase separation occurs during deposition. Diffusional transport during deposition is confined to the film surface, in accordance with our previous conclusions from experimental observations of Al-Ge thin films. We find that the lateral scale of the compositionally distinct domains formed by phase separation increases with film thickness to a steady-state size which varies with the ratio of the interdiffusion coefficient to deposition rate. The results are compared with theoretical predictions[11] and experimental observations.[13]

II. SIMULATION PROCEDURE

Surface interdiffusion is the underlying mechanism of the phase separation process we consider in our simulations. Since diffusion occurs by a random walk process, diffusional phase separation may be accurately modeled with Monte Carlo methods. In addition, our previous experimental observations of Al-Ge thin films,[13] coevaporated over a range of deposition temperatures, are consistent with the assumption that phase separation during deposition is controlled by surface interdiffusion; therefore, our simulations restrict the phase separation process to the film surface. In this model, the bulk of the film is frozen and a cross section through the film thickness provides a history of the microstructure that previously existed at the film surface, before it was buried through continued deposition. We refer to this as the frozen bulk approximation.

Since a solid surface contains of order 10^{15} atoms/cm^2, a simulation of phase separation which follows the motion of the atoms in an area as small as 1 μm^2 would ordinarily require monitoring approximately 10^{10} atoms for a 10^3-Å-thick film. Previous experimental results[13] showed that a typical length scale for the domains of a phase-separated Al-Ge thin film (50 vol % Al) coevaporated at 200 °C is ~0.3 μm [see Fig. 1(a)]. Therefore, to simulate a microstructure containing 100 domains, we would need to consider an area on the order of 10 μm^2, which would require monitoring the motion of 10^{11} atoms in a 10^3-Å-thick film. A typical time step in molecular-dynamics simulations is 10^{-14} s, i.e., simulating a typical experiment of 1 h would require approximately 10^{17} time steps. Since following the trajectories of 10^{11} atoms for 10^{17} time steps is beyond the scope of even the fastest computers currently available, we employ a model that is based on cells whose dimensions are of microstructural length scales. We map the film microstructure onto discrete lattice sites of a simple cubic lattice, such that each site represents a volume of material from the real microstructure. Deposition is incorporated by adding randomly mixed two-component layers of material to the film surface at regular time intervals. The time between the deposition of any two layers establishes the deposition rate. Since the film surface

is assumed to remain flat, this simulation procedure is applicable only when the roughness of the real film is small compared with the microstructure-scale thickness of each added layer. A similar approach has been successfully applied to simulate columnar microstructure development in single-phase thin films.[5–8]

Each lattice site in the simulation is assigned either a 1 or -1 to represent the components of a binary thin film. These lattice point labels are referred to as spins in reference to the terminology borrowed from magnetic Ising model simulations (see, e.g., Ref. 14). The simulations begin by filling a $3\times N\times N$ lattice with spins of random sign such that each of the three layers has the overall film composition. In order to minimize the effects of edges in the simulation, periodic boundary conditions are maintained within each of the $N\times N$ layers, and the lattice dimension N is set large enough to ensure that the results are independent of its magnitude. Typically, the simulations are performed with the lattice dimension N equal to 100, 200, or 300.

After depositing the first three layers of the film, as described in the preceding paragraph, the microstructure is allowed to evolve. We simulate phase separation through surface interdiffusion by attempting to exchange spins at two sites within the two most recently deposited layers of the film. Site selection is performed as follows: The first site is randomly selected from the topmost layer and the second is chosen randomly from within a volume of neighboring sites surrounding the first site selected. We chose to allow equally weighted exchange attempts between the site in the topmost layer and all of the 17 first ($\langle 100\rangle$), second ($\langle 110\rangle$), and third ($\langle 111\rangle$) -nearest-neighbor sites of the simple cubic lattice surrounding this site.

The change in energy of the system that would result from the hypothetical exchange of two neighboring spins is determined using the Ising Hamiltonian for the energy of site i:

$$E_i=-\frac{J}{2}\sum_j(\delta_{s_i,s_j}-1), \tag{1}$$

where the sum is over all 17 (first, second, and third) neighbors (see preceding paragraph) of site i, $\delta_{a,b}$ is the Kronecker delta, s_i and s_j are the spins occupying sites i and j, and J is an arbitrary positive constant that sets the strength and sense of the interaction between unlike pairs of spins. J is set equal to $+1$ to simulate a system with limited miscibility. A large number of neighbors are included in the interaction range to reduce surface energy anisotropy.[15] Kawasaki spin-exchange dynamics[16] are employed, such that the probability $P(\Delta E)$ of an exchange being accepted is given by

$$P(\Delta E)=\frac{\exp(-\Delta E/k_BT)}{1+\exp(-\Delta E/k_BT)}, \tag{2}$$

where $\Delta E=E_{\text{new}}-E_{\text{old}}$, and E_{new} and E_{old} are the respective energies of the lattice after and before a hypothetical site exchange, k_B is Boltzmann's constant, and T is the simulation temperature, defined in units of J/k_B. All of the simulations discussed here were performed at a temperature of $5J/k_B$, which corresponds to approximately $\frac{1}{4}$ the critical temperature for bulk phase separation in this model for equal concentrations of 1's and -1's. The entire process of selecting a pair of sites, calculating the change in energy that would result from their exchange, and accepting the exchange with probability $P(\Delta E)$, is repeated a large number of times such that each spin has a large number of exchange opportunities. Following each of these "diffusional" microstructural development cycles, a new random monolayer is added at the film surface, and the entire process is repeated until a film of the desired thickness is grown.

The basic unit of time in the simulations is the Monte Carlo step per site (MCS), which corresponds to the time required to make N×N exchange attempts. By using Eq. (2) to determine the probability of accepting a particular exchange, the effect of an activation barrier to diffusion Q has been factored out of the simulations. The jump rate for diffusion is obtained by multiplying $P(\Delta E)$ by $\exp(-Q/k_BT)$. Thus, in addition to changing $P(\Delta E)$ in Eq. (2), the effect of changing temperature on the simulations is a rescaling of simulation time (in MCS) relative to the actual time elapsed in a laboratory experiment. τ, the number of MCS between the addition of new random monolayers, of thickness a_0, to the growing film, sets the velocity of advance of the film surface v as a_0 per τ MCS. In these simulations, deposition rates between 2×10^{-4} and 10^{-1} a_0/MCS were considered. The lattice constant a_0, serves as the basic unit of length for all measurements made in the simulations. Finally, the results are averaged over five independent simulation runs for each set of deposition conditions.

The number of diffusive jumps made by a spin on the film surface before it is buried by the next layer is proportional to $\tilde{D}_s\tau$, where $\tilde{D}_s$ is the surface interdiffusion coefficient. Therefore, the simulation results depend only on $\tilde{D}_s\tau=\tilde{D}_s\delta/v$, where δ is the thickness of the surface layer in which interdiffusion occurs. We later show that a convenient length scale for interpreting the simulations, which appears naturally in the theoretical model[11] on which the simulations are based, is given by

$$\rho=\sqrt{\tilde{D}_s\delta/v}. \tag{3}$$

ρ can be interpreted as the interdiffusion distance during the deposition of a layer of thickness δ. The only temperature dependence in Eq. (3) is that of $\tilde{D}_s$. Therefore, both raising the temperature and decreasing the deposition rate will increase the interdiffusion distance. In order to avoid complications resulting from making an arbitrary choice for the activation energy, we chose to control the phase separation process by altering v rather than the simulation temperature.

III. RESULTS

The procedure outlined in the previous section was used to simulate phase separation during the growth of thin films with average compositions of 10 and 50 vol %

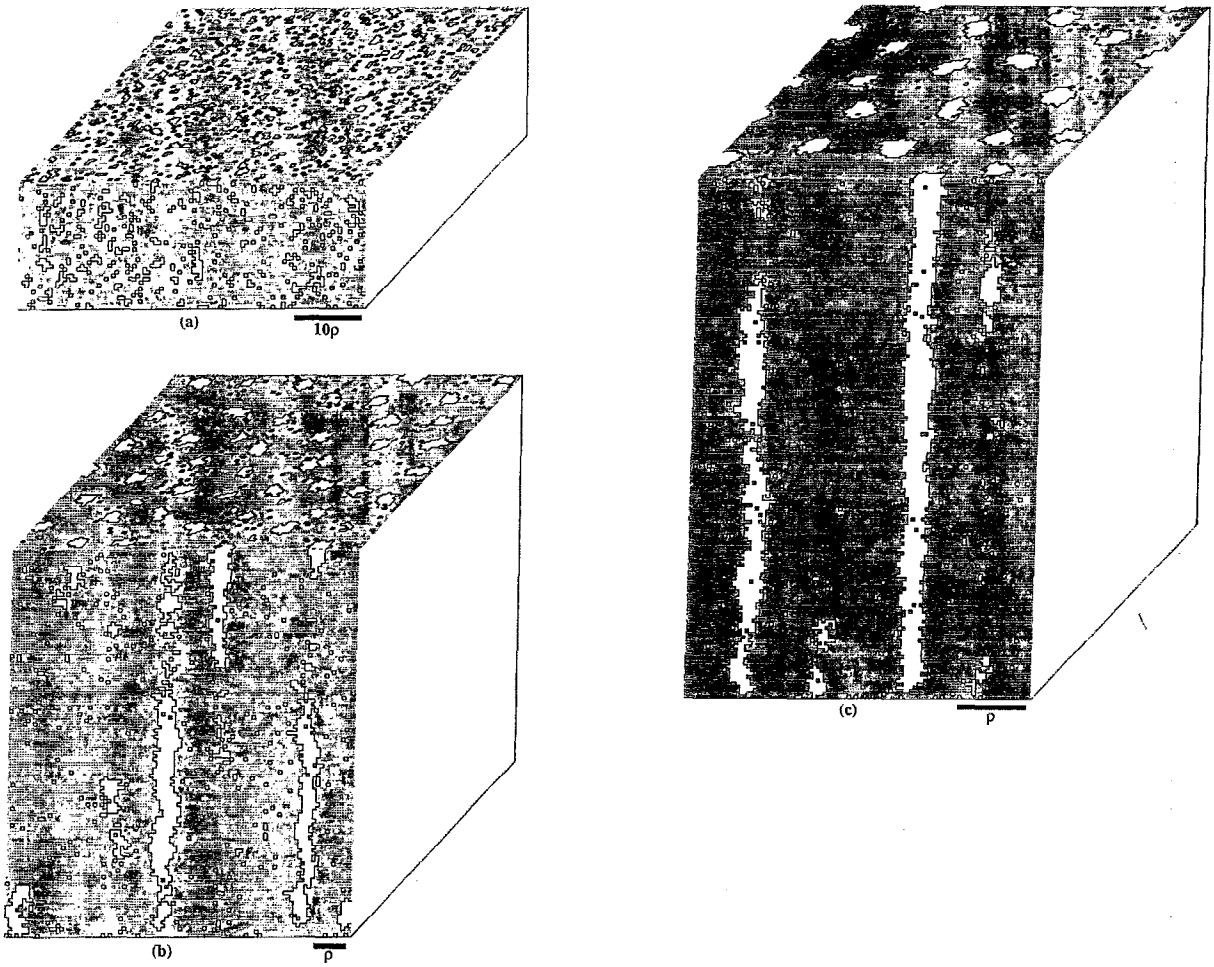

FIG. 2. Perspective views showing cross sections through, and surface microstructure of, simulated films containing 10 vol % solute codeposited at (a) 10^{-1}, (b) 5×10^{-3}, and (c) 1×10^{-3} a_0/MCS. The cross sections show the entire film thickness from substrate to film surface. ρ is the surface interdiffusion distance determined using Eq. (3).

solute (the phase diagram is symmetric about 50 vol %). The microstructures obtained at these two compositions exhibit distinctly different domain morphologies. Perspective views, showing the domain morphology at both the film surface and a cross section perpendicular to the film surface, for three deposition rates, are presented in Figs. 2 and 3 for simulations at 10 and 50 vol % solute, respectively. The solute-rich domains of the 10 vol % films form uniformly sized and spaced, nearly cylindrical, columns extending from the substrate to the film surface. These solute-rich domains, α, are separated from one another by a solvent-rich matrix phase β. At 50 vol %, the domain morphology at the film surface consists of a network of extended open domains reminiscent of a ferromagnetic Ising microstructure.[14] At both film compositions, the majority of the domain evolution during growth occurs within the first few deposited layers of each film, after which the domain morphology appears to approach a steady state. At the fastest deposition rate, where the diffusion distance ρ is comparable to the lattice spacing, steady state is achieved through the nucleation and growth of new domains throughout film deposition. Each of these simulations was allowed to progress until no further domain evolution was apparent at the film surface with continued deposition. The cross sections in Figs. 2 and 3 show the entire thickness of the deposited films.

The scale markers in the figures are a measure of the mean interdiffusion distance ρ calculated using Eq. (3). Assuming a random-walk diffusion process, the interdiffusion coefficient $\tilde{D}_s$ was calculated using[17]

$$\tilde{D}_s=(\tfrac{6}{17})a_o^2\Gamma, \tag{4}$$

where the exchange attempt frequency Γ is 1 $(\mathrm{MCS})^{-1}$, and six out of the possible 17 exchanges with neighboring sites result in motion having a component in one of the in-plane lattice directions. At either alloy composition, the calculated interdiffusion distances at the fastest deposition rates are comparable to the scale of the domain size. The rate of increase in domain size at the film surface with decreasing deposition rate is slower than the corresponding rate of increase in the random-walk interdiffusion distance (see below).

Visual examination of the surfaces of the simulated microstructures presented in Figs. 2 and 3 suggests the

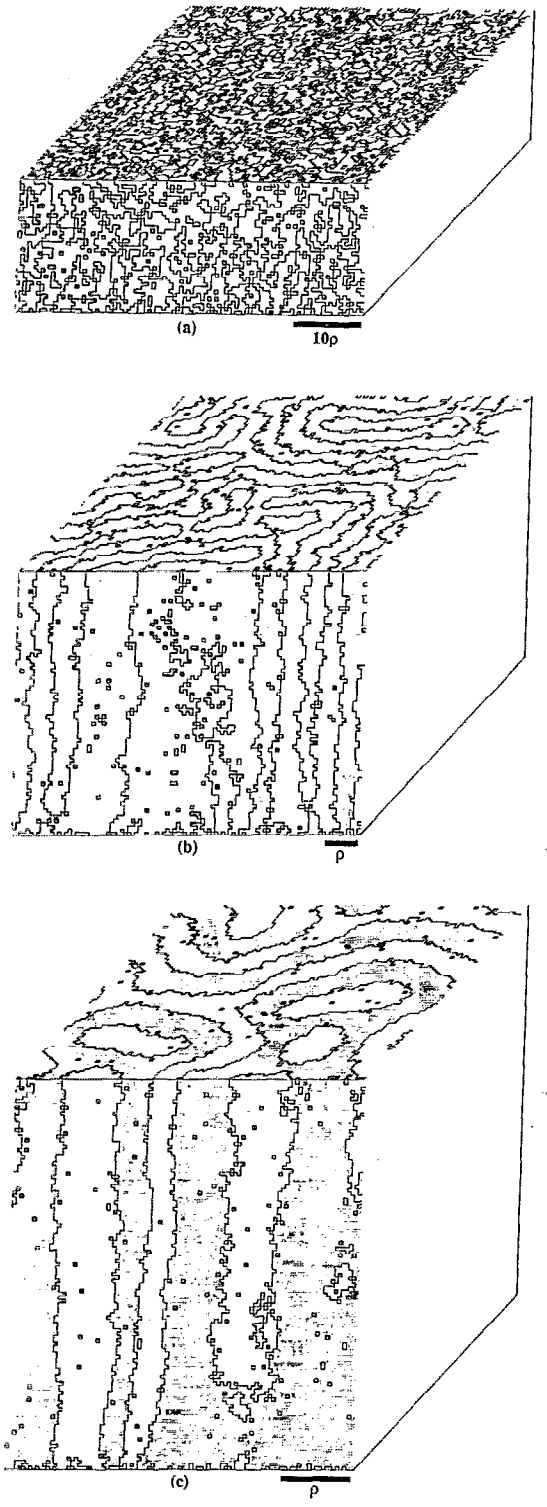

FIG. 3. Same as Fig. 2 for a film composition of 50 vol % solute.

solute domain size distributions are bimodal. In fact, measurement of the distribution of domain areas (number of lattice sites contained within a cross section through a domain and parallel to the film plane) for each layer of the 10 vol % films substantiates this observation (see Fig. 4). The very small domains can be associated with equilibrium solubility, solute trapping, or the intersections of shrinking domains with the film layer of interest. By examining the

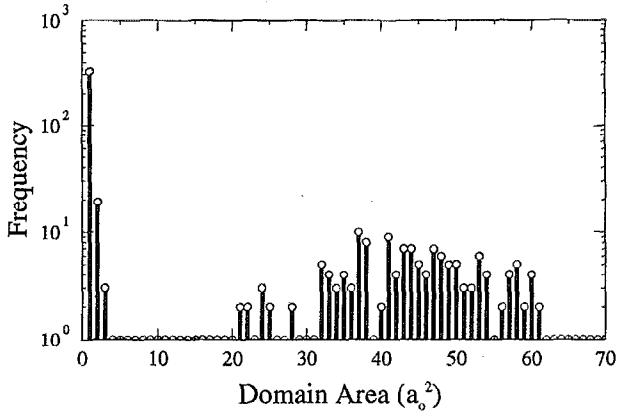

FIG. 4. Steady-state domain size (area) distribution in a simulated, co-deposited, film containing 10 vol % solute. The deposition rate was 2×10^{-3} a_0/MCS. Similar bimodal distributions were observed at other deposition rates.

domain morphology near the end of the simulations, when the films are close to a steady-state condition, we can conclude that few, if any, of these small domains are the tops of larger, shrinking, domains terminating at the film surface. Figure 5 shows the steady-state solute concentration in the majority phase, β, at the film surface as a function of deposition rate for films containing 10 vol % solute. Isolated solute atoms, as well as those contained in doublets and triplets, were counted for this purpose. The dashed line drawn in the figure is the equilibrium bulk solubility in the β phase c_β^0 ($=1-c_\alpha^0$ since the phase diagram is symmetrical about the 50 vol % composition) at the simulation temperature, as determined for a regular solution at small solute concentrations:[18]

$$c_\beta^0=\exp(-zJ/k_BT). \tag{5}$$

In this simulation $z=26$, the number of sites with which a site in the bulk of the film interacts. As the deposition rate decreases, the solute content in the β domains approaches c_β^0. Therefore, we conclude that the β domain solute con-

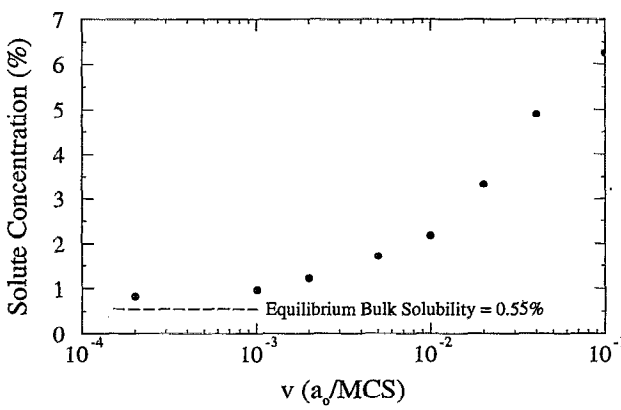

FIG. 5. Steady-state solute concentration in the majority phase, β, at the film surface as a function of deposition rate v for films containing 10 vol % solute.

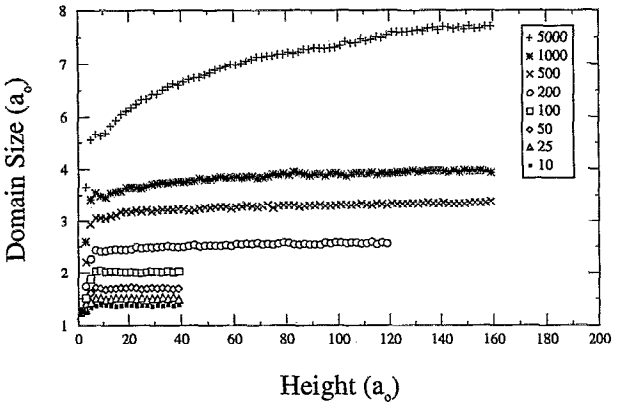

FIG. 6. α domain size $[(\text{area}/\pi)^{1/2}]$ at the film surface as a function of film thickness in simulated, codeposited, films containing 10 vol % solute. The time ($\tau = 1/v$) in MCS between the deposition of successive film layers is indicated in the legend.

tent in excess of c_β^0 is the result of solute trapping due to the imposition of a finite deposition rate and the frozen bulk approximation.

Domain evolution with film thickness was monitored by measuring the average domain size within each film layer. For the 10 vol % films, this meant counting the number of lattice sites contained within each α domain to determine an average domain area A in each film layer. Since these relatively compact domains are nearly circular in cross section, the square root of domain area normalized by π, $(A/\pi)^{1/2}$, is used as a measure of their size. At 50 vol % either phase can be considered the solute-rich phase and the domains are no longer simple closed shapes, but span the entire lattice. As a result, the domain area is effectively infinite and we therefore use the mean chord length in two orthogonal directions as a measure of the average domain size within each film layer. Domains corresponding to equilibrium and trapped solute were excluded from the average domain size calculations for both film compositions. The resultant domain size versus film thickness plots for the range of deposition rates considered are shown in Figs. 6 and 7 for 10 and 50 vol % films, respectively. Each curve is the average of five independent simulations. Note that, for all deposition rates and both compositions, the domain size increases very rapidly during the initial stages of growth (within approximately the first ten layers of the films) followed by a much slower approach to a steady state. As the deposition rate is reduced, the value of the steady-state domain size increases, as do the total film thickness and simulation time necessary to reach steady state.

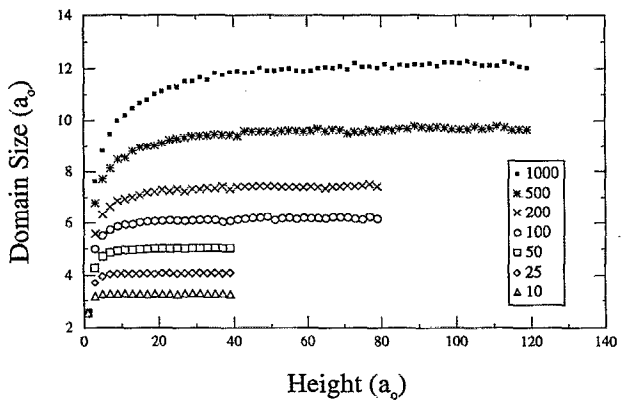

FIG. 7. Domain size (mean chord length) at the film surface as a function of film thickness in simulated, codeposited, films containing 50 vol % solute. The time ($\tau = 1/v$) in MCS between the deposition of successive film layers is indicated in the legend.

Additional simulations were performed to determine if the steady-state domain size approached at large film thicknesses is a true steady state. The steady-state microstructure obtained at a particular deposition rate was used as the starting configuration for further film growth at a second deposition rate. The resultant domain size after reaching a second steady-state condition was the same as if the film had been grown from the start at the second deposition rate. Therefore, we believe the steady-state domain size achieved at each deposition rate is independent of initial domain morphology and unique to each deposition rate.

IV. DISCUSSION

The simulation results may be directly compared with our experimental observations of phase separation in coevaporated Al-Ge thin films.[13] As discussed in Sec. I, phase separation is expected during coevaporation of Al-Ge thin films that have overall compositions within the two-phase region of the phase diagram. The surface morphologies observed in Figs. 1(a) and 1(b) are similar to those obtained in simulations performed at the same film composition of 50 vol % solute (Fig. 3). In particular, the surface of the Al-Ge film deposited at 200 °C [Fig. 1(a)] is characterized by an arrangement of serpentine, open domains which span the film surface. At 375 °C [Fig. 1(b)], the domains are more compact, yet still irregularly shaped. Examination of the simulated thin-film microstructures presented in Figs. 2 and 3 shows that the phase morphology at the film surface is representative of the underlying bulk microstructure of the films. This observation is also consistent with our comparison of SEM photomicrographs of coevaporated Al-Ge film surfaces with the bulk microstructures observed in plan-view and cross-sectional transmission electron microscopy (TEM).[13] We note that SEM examination of an Al-Ge film deposited at 375 °C showed the scale of the surface roughness of this film was comparable to the film thickness. Therefore, the notion that the film surface remains flat throughout deposition, as assumed in the theoretical[11] and simulation models, is not valid for high-temperature deposition.

Qualitative similarities between the simulation and experimental results are also evident in the effect of deposition temperature and deposition rate on phase separation. Increasing ρ [see Eq. (3)] by lowering the deposition rate in simulations, or raising the temperature in experiments, led to an increase in domain size.

While grain boundaries are clearly visible in the SEM micrograph presented in Fig. 1(b), the present simulations did not account for the polycrystalline nature of physical vapor-deposited thin films. The grain boundaries in the Al domains are straight and traverse the domains at necks, suggesting that the grain boundaries are in metastable equilibrium with domain boundaries for the domain size achieved. Second, if the grain-boundary energy were larger than the domain boundary energy, we would expect to find deep grooves along grain boundaries at triple junctions where two Al grains meet a Ge domain. Since this is not observed [see Fig. 1(b)], we believe it is the phase separation process, as opposed to grain growth, which determines domain size and shape. Therefore, we do not expect the absence of grain boundaries in the simulations to significantly affect domain evolution.

The simulation results may also be compared with the theoretical predictions.[11] The theoretical model assumes, as does the simulation model, that phase separation during film growth is controlled by surface interdiffusion, and that bulk interdiffusion is negligible. In this limit, the bulk of the film provides a history of the microstructure that existed at the film surface before the surface was buried by the continuous deposition flux. Intuitively, the imposition of this frozen bulk approximation and a finite deposition rate demand that a steady-state domain size be approached during deposition, as shown in Figs. 6 and 7. Any given layer of the film is at the surface for a finite time period, determined by the deposition rate v, and subsequently becomes part of the frozen bulk. Therefore, the surface interdiffusion distance ρ also depends on v [see Eq. (3)]. As a result, domains cannot grow indefinitely and ultimately reach a steady-state size. Our experimental observations of coevaporated Al-Ge thin films[13] are consistent with this picture of the phase separation process. We found the temperature dependence of the steady-state domain size in these films to be consistent with surface interdiffusion controlled phase separation.

The theoretical model[11] is based on the idealized microstructure shown in Fig. 8. It consists of cylindrical α domains of steady-state radius R_∞ separated by an average distance $2\Re$ and surrounded by continuous regions of a second phase, β. This microstructure is very similar to the simulated microstructures obtained for low solute concentrations (Fig. 2). At the film surface, the diffusion equation applicable to the phase separation process leading to this microstructure is given by

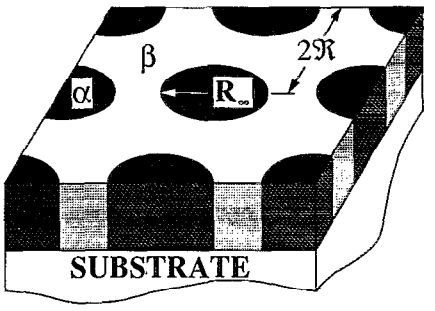

FIG. 8. Idealized domain structure of a laterally phase-separated film as assumed in the theoretical model for phase separation of Ref. 11.

$$\frac{\partial c}{\partial t}=\tilde{D}_s\nabla_s^2 c+\frac{v}{\delta}(c_0-c), \tag{6}$$

where c_0 is the composition of the incoming vapor flux, and the surface Laplacian $\nabla_s^2=(\partial^2/\partial x^2+\partial^2/\partial y^2)$ for the flat film surfaces considered here. The theoretical model predicts a steady-state ($\partial c/\partial t=0$) domain size, but does not describe the approach to steady state. To do so, factors such as the initial distribution of nuclei or the nucleation rate, the solute composition profiles within the nuclei, and the effects of domain coalescence during film growth would need to be considered. The steady-state composition profiles obtained as solutions to Eq. (6) inside and outside an α domain are presented in Ref. 11. Application of mass conservation to these composition profiles gives the following transcendental relationship between the interdiffusion distance ρ, the steady-state domain radius R_∞, and $\Re$:

$$\frac{c_\alpha^0-c_0}{c_0-c_\beta^0}=\frac{[I_1(\Re/\rho)K_1(R_\infty/\rho)-K_1(\Re/\rho)I_1(R_\infty/\rho)]I_0(R_\infty/\rho)}{[K_0(R_\infty/\rho)I_1(\Re/\rho)+I_0(R_\infty/\rho)K_1(\Re/\rho)]I_1(R_\infty/\rho)}, \tag{7}$$

where c_α^0 and c_β^0 are the equilibrium compositions of coexisting α and β phases obtained at the α-β interface neglecting the effects of capillarity, and I_n and K_n are modified Bessel functions of the first and second kind, respectively, of order n. If c_0 is sufficiently close to c_β^0 (a dilute alloy) that $\Re/R_\infty \gg 1$ and $R_\infty \approx \rho$, then $\Re/\rho \gg 1$ and Eq. (7) reduces to

$$\frac{c_\alpha^0-c_0}{c_0-c_\beta^0}=\frac{K_1(R_\infty/\rho)I_0(R_\infty/\rho)}{I_1(R_\infty/\rho)K_0(R_\infty/\rho)}. \tag{8}$$

For a given film composition c_0, the left-hand side of Eq. (8) is fixed and the ratio R_∞/ρ is a constant. Using this result and Eq. (3), Atzmon and co-workers[11] obtain

$$R_\infty \propto \sqrt{D_s\delta/v}. \tag{9}$$

With the above assumptions, the theory predicts the steady-state domain radius R_∞ to be proportional to $(1/v)^{1/2}$. In Fig. 9 we plot the steady-state domain size determined from Figs. 6 and 7 ($c_0=10$ and 50 vol %, respectively) against the reciprocal of deposition rate ($1/v$). For both film compositions, these curves are well described

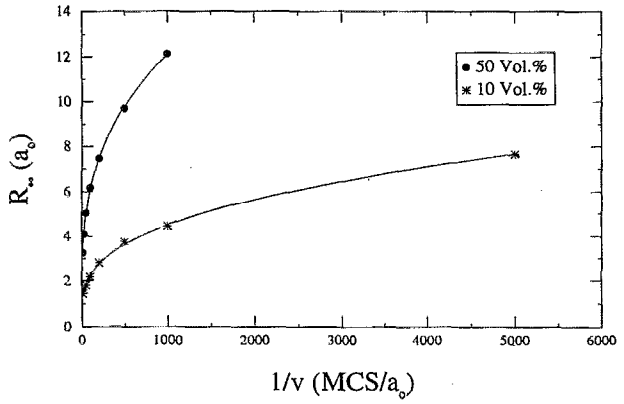

FIG. 9. Mean steady-state domain size at the surface of simulated codeposited films containing 10 vol % solute [$R_\infty = (\text{area}/\pi)^{1/2}$] and 50 vol % solute ($R_\infty$ = mean chord length) as a function of the reciprocal of deposition rate ($1/v$). The curve drawn through the data points is a least-squares power-law fit to the data with an exponent of 0.37 at 10 vol % and 0.33 at 50 vol %.

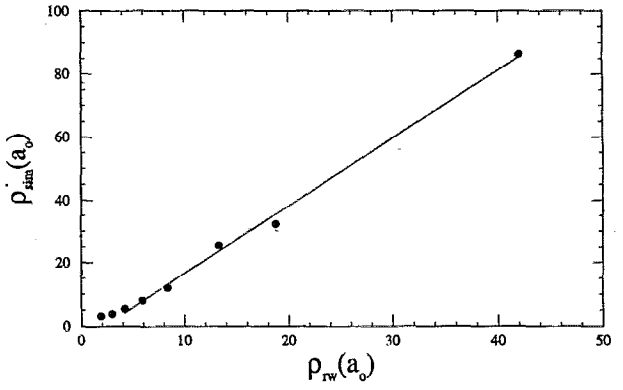

FIG. 10. Random-walk interdiffusion distance ρ_{rw} plotted against the interdiffusion distance determined from simulations and Eq. (7) (ρ_{sim}) for films containing 10 vol % solute. The curve drawn through the data is a least-squares linear fit (slope=2.15) to all the data points except the two at the smallest interdiffusion distances.

by power laws [$R_\infty = B(1/v)^n$, where B and n are constants]. The exponents obtained (0.33 ± 0.01 for $c_0 = 50$ vol % and 0.37 ± 0.02 for $c_0 = 10$ vol %) are different from one another and neither equals the theoretically predicted exponent of $\frac{1}{2}$.

If the data presented in Fig. 9 were obtained from films of thickness less than that required to attain steady state at the film surface, the exponents determined from power-law fits of the data would be lowered systematically. However, this is not a likely resolution of the disagreement between the exponents obtained from the simulations and that expected theoretically since the average increase in domain size in the last ten layers added to each film was in all cases $\leqslant 0.1\%$ of the steady-state domain size. In addition, we found that the steady-state domain size achieved is independent of the initial domain size and distribution. Therefore, we believe the data presented in Fig. 9 are derived from films that have achieved a true steady state.

The theoretical model which led to Eq. (9) assumes that c_0 is sufficiently close to the equilibrium solid solubility of the β phase c_β^0 that $\Re/R_\infty \gg 1$ and also that $R_\infty \approx \rho$, such that $\Re/\rho \gg 1$. In Table I the values of R_∞ determined from Fig. 6 and estimates of $\Re$ and ρ are presented for each of the deposition rates in the simulations for $c_0 = 10$ vol %. Values of $\Re$ were obtained from the following: $N^2/m = \pi\Re^2$, where N is the size of the simulation lattice and m is the average number of α domains per film layer excluding those attributable to equilibrium solubility or solute trapping. Of the two columns of ρ values presented in the table, those under the heading of "random walk" were obtained using Eq. (3) and the random-walk interdiffusion coefficient given by Eq. (4). The ρ values in the column labeled "simulation" were obtained from numerical solutions to Eq. (7) using $\Re$ and R_∞ values determined from the simulations. It is clear from the table that the assumption $\Re/R_\infty \gg 1$ is not valid at any deposition rate for this composition. Therefore, the $\frac{1}{2}$ power-law dependence that results from the assumptions of Ref. 11 [Eq. (9)] is inapplicable.

TABLE I. Comparison of the surface interdiffusion distance ρ, steady-state domain size R_∞, and one-half the interdomain spacing $\Re$ at various deposition rates for films containing 10 vol % solute. Distances are expressed in terms of the lattice constant a_0.

Deposition rate v (a_0/MCS)	Avg. domain size R_∞ (a_0)	Avg. domain spacing/2 ($\Re$) (a_0)	Interdiffusion distance ρ (a_0)	
			Random walk	Simulation
0.1	1.44	5.38	1.88	3.17
0.04	1.59	5.52	2.97	3.80
0.02	1.80	5.64	4.20	5.43
0.01	2.18	6.55	5.94	8.07
0.005	2.82	8.33	8.40	11.96
0.002	3.75	10.75	13.32	25.55
0.001	4.45	12.73	18.79	32.30
0.0002	7.66	21.72	42.01	86.40

In Fig. 10 the random-walk interdiffusion distances are plotted against the interdiffusion distances determined from the simulations and numerical solutions to Eq. (7) for $c_0 = 10$ vol %. The ρ values determined from the simulations are in all cases larger than those obtained assuming random-walk interdiffusion. The curve drawn through the data is a least-squares linear fit to all the data points except the two at the smallest interdiffusion distances (fast deposition rates), where we believe the interdiffusion distances determined from the simulations are unreliable since they are comparable to the resolution of the simulation lattice. It is gratifying to observe a nearly proportional relationship between the two independently determined values of ρ. The slope of the line (2.15 ± 0.07) can be interpreted as the square root of the thermodynamic factor (Ref. 17, p. 140) relating the random-walk interdiffusion coefficient to the chemical interdiffusion coefficient.

For the simulations performed at $c_0 = 50$ vol %, the criterion $\Re/R_\infty \gg 1$ is obviously not satisfied (see Fig. 3). The α and β domain sizes are comparable and therefore $\Re \approx R_\infty$. In addition, the domain morphology of the sim-

ulated films is very different from that of the idealized microstructure on which the theoretical model is based (Fig. 8). Therefore, the theory is inapplicable to this situation. We point out that the power-law exponent that is observed (0.33) is the same as that expected from the analysis of Lifshitz and Slyozov[19] and Wagner[20] (LSW) for precipitate coarsening in two dimensions. However, the LSW exponent of $\frac{1}{3}$ is expected only in the limit of zero α volume fraction and is not appropriate to our simulations in which new material is added to the system. The diffusion equation used in the LSW theory must be replaced by that in Eq. (6) to account for deposition. Also, in contrast to the presently modeled process, LSW coarsening is driven exclusively by capillary forces and the domain size at a given time is strongly dependent on the initial conditions. We therefore conclude that the agreement between our exponent and that of LSW theory is coincidental.

Although we have performed simulations at only two compositions, we find that the exponent obtained for the power-law variation in steady-state domain size with the reciprocal of deposition rate increases from 0.33 ± 0.01 to 0.37 ± 0.02 as the film composition decreases from 50 to 10 vol %. We therefore speculate that the theoretically predicted exponent of $\frac{1}{2}$ will only be observed in the limit that the volume fraction of α domains in the film approaches zero, which is consistent with an average film solute content approaching the equilibrium solid solubility curve for the majority β phase.

Finally, although the imposition of a fixed deposition rate within the frozen bulk approximation limits the interdiffusion distance, a second factor may determine the steady state that is achieved. For example, Cahn assumed in his analysis of eutectoid decomposition[12] that the steady-state lamellar spacing was determined by the minimization of free energy—the reduction in interfacial free energy with increasing lamellar spacing is balanced by the increase in bulk free energy with increasing supersaturation as lamellar spacings increase. If we assume, as Cahn did, that the variation in the free energy of the supersaturated solid solution with composition is parabolic, application of this free-energy minimization criterion in a lamellar geometry suggests that the steady-state lamellar thickness should be proportional to $(1/v)^{2/5}$.[11] This exponent is close to the exponent of 0.37 ± 0.02 that was obtained from the simulations performed for $c_0 = 10$ vol %. However, the theoretically predicted value of this exponent depends strongly on the form of the free-energy variation with composition assumed for the supersaturated solid solution and we believe this agreement to be fortuitous.

V. SUMMARY

We have successfully applied Monte Carlo methods to the simulation of phase separation during codeposition of thin films in the limit of negligible bulk diffusion (the frozen bulk approximation). The microstructures developed at low solute concentrations are columnar, consisting of uniformly sized and spaced cylindrical domains embedded in a second phase. The domains evolve through surface interdiffusion during deposition to a steady-state size R_∞, which is independent of initial conditions. For films having a composition of 50 vol % solute, the microstructures obtained in the simulations are similar in appearance to those of coevaporated Al-Ge films of the same composition.

The variation of R_∞ with $\tilde{D}_s/v$ agrees qualitatively with a previously developed theoretical model, which predicts the steady-state domain size at low solute concentrations is proportional to $\rho = (\tilde{D}_s \delta / v)^{1/2}$. However, the exponent obtained from the power-law variation of R_∞ with $1/v$ for simulations at 10 vol % is 0.37 ± 0.02 instead of the theoretically predicted value of $\frac{1}{2}$. We attribute this difference to the fact that the assumptions in the theoretical model apply to different deposition conditions than those examined in the present simulations. The value of the surface interdiffusion distance during deposition, determined using our previous theoretical model, agrees with that calculated from first principles for the present simulation, assuming the interdiffusion coefficient to be approximately 4.6 times its random-walk value.

ACKNOWLEDGMENTS

This project was funded in part by the National Science Foundation, Grant No. DMR-9200932 and the Air Force Office of Scientific Research, Grant No. AFOSR-90-0112. The authors gratefully acknowledge the helpful suggestions provided by Dr. G. S. Grest during the course of this work.

[1] R. W. Cahn and P. Haasen, *Physical Metallurgy* (North-Holland, Amsterdam, 1983).
[2] B. A. Movchan and A. V. Demchishin, Phys. Met. Metallogr. **28**, 83 (1969).
[3] J. A. Thornton, J. Vac. Sci. Technol. **11**, 666 (1974).
[4] J. A. Thornton, J. Vac. Sci. Technol. **12**, 830 (1975).
[5] D. J. Srolovitz, A. Mazor, and B. G. Bukiet, J. Vac. Sci. Technol. A **6**, 2371 (1988).
[6] D. J. Srolovitz, J. Vac. Sci. Technol. A **4**, 2925 (1986).
[7] A. Mazor, D. J. Srolovitz, P. S. Hagan, and B. G. Bukiet, Phys. Rev Lett. **60**, 424 (1988).
[8] S. Ling and M. P. Anderson, J. Electron. Mater. **17**, 459 (1988).
[9] K.-H. Müller, J. Appl. Phys. **58**, 2573 (1985).
[10] P. Meakin, P. Ramanlal, L. M. Sander, and R. C. Ball, Phys. Rev. A **34**, 5091 (1986).
[11] M. Atzmon, D. A. Kessler, and D. J. Srolovitz, J. Appl. Phys. **72**, 442 (1992).
[12] J. W. Cahn, Acta Metall. **7**, 18 (1959).
[13] C. D. Adams, M. Atzmon, Y.-T. Cheng, and D. J. Srolovitz, J. Mater. Res. **7**, 653 (1992).
[14] G. S. Grest and D. J. Srolovitz, Phys. Rev. B **30**, 5150 (1984).
[15] E. A. Holm, J. A. Glazier, D. J. Srolovitz, and G. S. Grest, Phys. Rev. A **43**, 2662 (1991).
[16] K. Kawasaki, in *Phase Transitions and Critical Phenomena*, edited by C. Domb and M. S. Green (Academic, New York, 1972), Vol. 2.
[17] P. D. Shewmon, *Diffusion in Solids*, 2nd ed. (McGraw-Hill, New York, 1989).
[18] D. A. Porter and K. E. Easterling, *Phase Transformations in Metals and Alloys* (Van Nostrand Reinhold, Berkshire, 1981).
[19] I. M. Lifshitz and V. V. Slyozov, J. Phys. Chem. Solids **19**, 35 (1961).
[20] C. Wagner, Z. Elektrochem. **65**, 243 (1961).